Can a starting vortex boost the turbulent transition of a Richtmyer-Meshkov instability-induced air/helium mixing zone?

Marta Rasteiro dos Santos, Yannick Bury, Pierre Graumer, Stéphane Jamme

Can a starting vortex boost the turbulent transition of a Richtmyer-Meshkov instability-induced air/helium mixing zone?

M. Santos, Y. Bury, P. Graumer, S. Jamme
ISAE-SUPAERO, Université de Toulouse, 31000 France

Corresponding Author's name: yannick.bury@isae-supaero.fr

Abstract

This work is part of the study of the turbulent mixture produced by the Richtmyer-Meshkov instability. It focuses on the characterization of the initial conditions and on their persistence when the mixing zone develops into a turbulent flow, in other words the so-called initial condition memory effect. A Direct Numerical Simulation of the flow arising from the rotation of series of blades initially separating two gases of different density is conducted. The analysis relies on the impact of the resulting vortical flow on the generation of a more or less diffused and disturbed initial gaseous interface as the rotational speed of the blades is varied. Results highlight different flow regimes, associated with the redistribution of the total vorticity between the different vortex cores promoted by the opening of the blades, as both the rotational speed and the gaseous medium in which the blade tips are moving into vary.

1 Introduction

The Richtmyer-Meshkov instability (RMI) is an hydrodynamic instability which occurs when an interface between two fluids with different densities is subjected to an impulsive acceleration, generally, a shock wave. This phenomenon can be observed when the core of a supernovae collapses and also in the reactions of Inertial Confinement Fusion (ICF). The first numerical studies were performed by Richtmyer[1] in 1960 while the first experimental observation was later reported by Meshkov[2] in 1969.

The underlying mechanism of the instability formation is the baroclinic torque. The pressure gradient at the shock wave discontinuity is responsible for the growth of the initial interface perturbation, generating a Richtmyer-Meshkov Instability-fueled flow. Its further evolution is governed by the vorticity transport equation:

$$\frac{D\boldsymbol{\omega}}{Dt} = \frac{1}{\rho^2}(\boldsymbol{\nabla}\rho \times \boldsymbol{\nabla}p) + (\boldsymbol{\omega}.\boldsymbol{\nabla})\mathbf{u} - \boldsymbol{\omega}(\boldsymbol{\nabla}.\mathbf{u}) + \nu\nabla^2\boldsymbol{\omega} \tag{1}$$

where ρ is the density, p is the pressure, ν is the viscosity, $\mathbf{u}$ is the velocity vector and $\boldsymbol{\omega}$ is the vorticity vector.

During the last forty years, various experimental facilities have been developed for the study of the Richtmyer-Meshkov instability. The latter allowed for a variety of different initial conditions. These conditions were first obtained with a physical separation between the two species, commonly a soft nitrocellulose membrane, for instance [2], [3]. Other solutions for the generation of a membraneless gaseous interface have been achieved only through the properties of the gas layers forming a gas curtain system [4] or a lateral co-flow system [5, 6]. Part of these studies allowed for the description of the macroscopic evolution of the spatio-temporal growth of the RMI instability for its three consecutive

regimes, namely the linear, non-linear and late-time [7]. Nevertheless, the precise description of the RMI-induced turbulent flow is not feasible due to the contamination of the test section when considering physical solid separation-induced initial conditions. The membraneless separation strategy establishes, *e.g.*, a falling gas interface as initial condition allowing to overcome this issue and quantifying the turbulent regime by means of the Reynolds stress tensor coming from instantaneous velocity and density fields [8]. Even if this configuration allowed to go a step further in the RMI-fueled flow characterization, the lack of a precise determination of the initial gas interface prevents to unveil whether the imprinted initial condition shape is preserved or not inside the mixing, especially in the turbulent regime.

Our research aims to decipher the memory of well-defined initial conditions and their effect during the turbulent transition and consecutive turbulent regime arising from a Richtmyer-Meshkov instability-fueled flow. For this purpose, an innovative experimental concept has been developed at ISAE-SUPAERO, based on a series of parallel rotating blinds initially separating two different gases at rest. Their sudden rotational opening generate a fully-controlled and weakly diffused initial gas interface (see Figure 1). In this paper, we analyze and discuss the DNS results of a parametric study on the rotational speed of these blades inside two stratified fluids of different densities. A detailed description of the flow promoted by this motion is not only useful for the full control of the RMI initial conditions but also interesting to uncover different flow configurations.

2 Basis concept of the initial condition generation

The experimental device which serves as the basis for this numerical study and which aims at the generation of the initial gaseous interface is a membraneless concept based on a series of rotating rectangular parallel blades. This device is inserted in the low pressure chambers of a vertical shock tube exploited at the ISAE-SUPAERO Fluid Dynamics laboratory. The two gas chambers (LP1 and LP2) are filled with air and helium (Atwood Number $A = 0.76$), respectively, and initially separated by a series of parallel blinds of rectangular shape disposed horizontally (closed device). The rapid opening of the blinds, from horizontal to vertical position, around a central pivot (corresponding to its axis of symmetry at $X = 0mm$) and according to an adaptable opening law ($\omega(t)$), generates a weakly diffused gas interface with limited molecular diffusion. The experimental device guarantees a high degree of repeatability and allows for a comprehensive description and control of the initial conditions in a reliable way. The numerical simulations presented in this work aim at the comprehensive characterization of the initial conditions obtained through different operating points of the device, corresponding to an opening time (t_{open}) adjustable from 1ms to 50ms.

3 Direct Numerical Simulations

We conducted a parametric study based on the main parameter of influence of the interface formation, the opening speed of the rotary blinds. As a first approach, we propose to decipher the dynamics of the flow arising from this complex geometry by eliminating the multi-species properties with mono-gas configuration. Then, the coupled effect of the dynamics of the flow and the species mixing is analyzed in a bi-gas air-helium configuration.

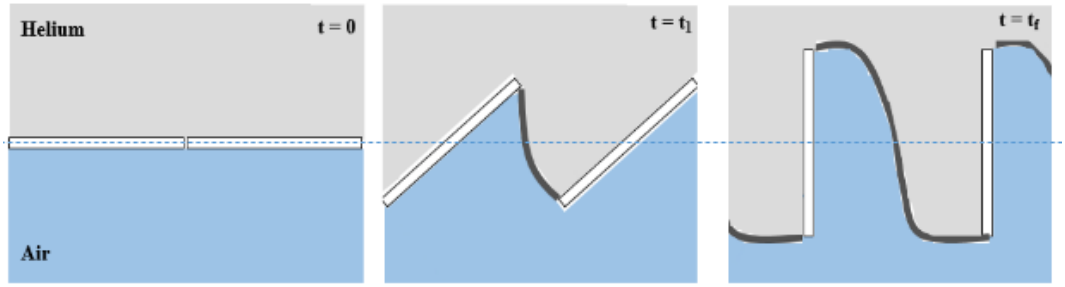

Fig.1 Illustration of the blade rotational motion from horizontal (left image) to vertical position (right image). The central image represents an instant t_1 of the blade's opening.

The two dimensional domain models the experimental low pressure chambers (LP1, LP2) and the multi blade device. For the mono-gas series of computations, LP1 and LP2 are filled with either air or helium. For the bi-gas configuration, LP1 is filled with air (blue in Figure 1) and LP2 is filled with helium (grey in Figure 1). The numerical model of the multi blade-based device, initially in the horizontal position separates LP1 and LP2 chambers. Due to numerical constraints, the domain width is reduced, representing only the three central blades of the experimental facility, with periodic boundary conditions at the lateral sides of the two chambers (note that for the sake of clarity, only two blades are illustrated on Figure 1). The 2D mesh is separated into a coarse region far away from the blades and a refined region in the zone surrounding the blades, accounting in a total of 280 000 quadrilateral cells. The coarse mesh base size is fixed to $1mm$ for the overall computational domain except in the vicinity of the blades where the refined mesh base size is fixed to $62.5\mu m$. The DNS computations accuracy is confirmed with a maximum cell-based Reynolds number of $Re_{mesh} = 31.334$ for the fastest blades rotational speed.

The blade's motion around its central pivot, depicted in Figure 1, is completed in a given time (t_{open}). Numerically, this is modelled as a rigid wall rotation inside the fluid domain driven by an opening law ($\omega(t)$). To accurately represent the physics of the problem, the opening law is decomposed into three consecutive phases: a constant accelerated motion phase ($\Delta t = 1\%$ of the t_{open}) at the beginning of the opening, a constant angular velocity motion phase ($\Delta t = 89\%$ of the t_{open}) applied during most of the opening and a constant decelerated motion phase ($\Delta t = 10\%$ of the t_{open}) at the end of the opening process. A second-order implicit scheme is used for the temporal discretization of the equations. The time-step is varied depending on the phase of the opening and on the opening speeds to maintain the same angular displacement at each time-step.

4 Vortex Tracking Method

The velocity fields resulting from the numerical computations were analyzed with an algorithm that detects and tracks the vortex structures. This code first identifies the vortex structures formed during the blade's rotational motion and then selects the relevant structures for tracking. The vortex identification is based on the $Qcriterion$ [9], in which the vortex cores are defined as connected regions ($\sum$) of positive Q. This method is extremely advantageous for the present flow analysis as it allows to highlight the starting vortex separation from the blade's tip and to calculate, at the same time, the quantitative

vortex properties. The vortex kinematic properties are computed as follows:

$$\Gamma = \iint_{\Sigma} \omega_z dxdy \tag{2}$$

in which ω_z is the out-of-plane vorticity at the vortex region $\sum$ and Γ is the vortex circulation.

The position of the vortex centroid, (x_c, y_c), is then calculated through the vortex circulation and it is given by:

$$\text{(a)}\ \ x_c = \frac{1}{\Gamma} \iint_{\Sigma} x\omega_z dxdy \qquad \text{(b)}\ \ y_c = \frac{1}{\Gamma} \iint_{\Sigma} y\omega_z dxdy \tag{3}$$

The two characteristic vortex core radii, respectively R_x R_y, can be defined based on the polar moments of vorticity as in [10]. The square root of the sum of the two square radii returns the vortex radius R. This values are then given by:

$$\text{(a)}\ \ R_x = \left[\frac{1}{\Gamma} \iint_{\Sigma} (x - x_c)^2 \omega_z dxdy\right]^{\frac{1}{2}} \qquad \text{(b)}\ \ R_y = \left[\frac{1}{\Gamma} \iint_{\Sigma} (y - y_c)^2 \omega_z dxdy\right]^{\frac{1}{2}} \tag{4}$$

$$R = \left[\frac{1}{2}(R_x^2 + R_y^2)\right]^{\frac{1}{2}} \tag{5}$$

5 Results and discussion

The analysis of the flow promoted by the opening of the blades relies on the spatio-temporal description of the so-generated vortical structures, as a function of the opening velocity and of the gaseous species located on both sides of the blades when initially closed. For both mono species (same gases in both LP1 and LP2 chambers) and bi-species configurations (pure air in LP1 chamber, pure helium in LP2 chamber), the total opening time of the blades is varied from 1 to $50ms$. At this stage of the discussion it is important to mention that, as a given blade is rotating, one of its tip will plunge into LP1 chamber while the other tip will ascend into LP2 chamber. For the bi-gas configuration, the flow around either the plunging or ascending tip will then develop differently, as a consequence of different fluid properties in LP1 and LP2 chambers, resulting in different local Reynolds numbers. The vortex parameters used for the analysis of the flow, described in section 4, are normalized based on the angular speed ω_{op}, the blade half length $R_{blade} = L/2$ (L is the width of the blade) and the properties - density ρ and dynamic viscosity μ - of the fluid contained in the chamber the tip of the blade is moving to. They are presented as a function of the Reynolds number $Re_{tip}^{LPi_{i=1,2}}$, as defined in equation (6b). For the mono gas configuration, it ranges from $Re_{tip}^{LP2_{i=1,2}} \approx 16$ (pure helium, $t_{open} = 20ms$) to $Re_{tip}^{LPi_{i=1,2}} \approx 2500$ (pure air, $t_{open} = 1ms$). For the bi-species configurations, the Reynolds number will have a different value at each blade tip since it is based on the density and

dynamic viscosity of the gas in which the plunging/ascending tip is moving (see definition in equation (6b)). It ranges between $Re_{tip}^{LP2} \approx 6.5$ (ascending tip in pure helium, $t_{open} = 50ms$) and $Re_{tip}^{LP1} \approx 2500$ (plunging tip pure air, $t_{open} = 1ms$).

$$\text{(a)}\ U_{tip} = \omega_{op} R_{blade} \qquad \text{(b)}\ Re_{tip}^{LPi_{i=1,2}} = \frac{\rho_i U_{tip} R_{blade}}{\mu_i} \tag{6}$$

where ρ_i is the density and μ_i is the dynamic viscosity of the gas in LPi chamber.

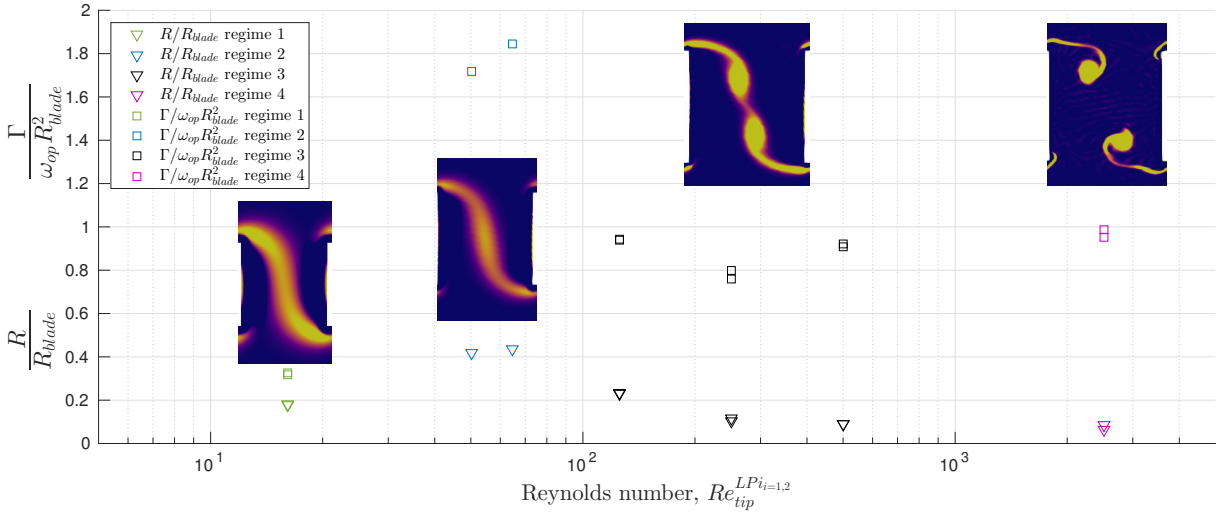

Fig.2 Normalized vortex circulation and radius as a function of the Reynolds number highlighting different flow regimes in a mono-gas configuration. Insert images depict iso contours of vorticity at the end of the rotational motion.

The synthesis of the results obtained for the mono-gas configuration and for $Re_{tip}^{LPi_{i=1,2}}$ ranging from 16 to 2500 are summarized in Figure 2. These results highlight the influence of the Reynolds number on the flow structure past the blades at the end of their rotational motion.

For very low Reynolds number ($Re \approx 16$), the shear layer initiated between the plunging and ascending blade tips remains connected to the blades, in the form of a weak and continuous, not uniformly distributed, vorticity layer. The vorticity level inside this layer tends to be more intense close to the blade tips, where two regions of positive Q criterion are identified. The latter should normally correspond to vortex cores. However it is important to mention that for this particular regime, namely regime 1, viscous forces dominate and tend to promote a solid rotation of the fluid volume surrounding the blades, which differ from the usual definition of a vortex core. For higher Reynolds number $Re_{tip}^{LPi_{i=1,2}} \approx 50$, the vorticity deposited between the blade tips cumulates into one single vortex structure, which position tends to remain fixed at mid distance between the plunging and ascending blade tips. In this regime, hereafter denoted regime 2, the main vortex circulation progressively increases as the Reynolds number is increased, until reaching a maximum close to $Re_{tip}^{LPi_{i=1,2}} \approx 64$, beyond which the split of this single vortex into two vortex structures, further denominated as starting vortices, causes the sudden decrease of both circulation and radius. For Reynolds numbers ranging between approx. 100 and 500, the flow exhibits new features. It is referred to as regime 3 on Figure 2. Here, the two starting vortices depict similar radius and circulation, with well-defined vortex

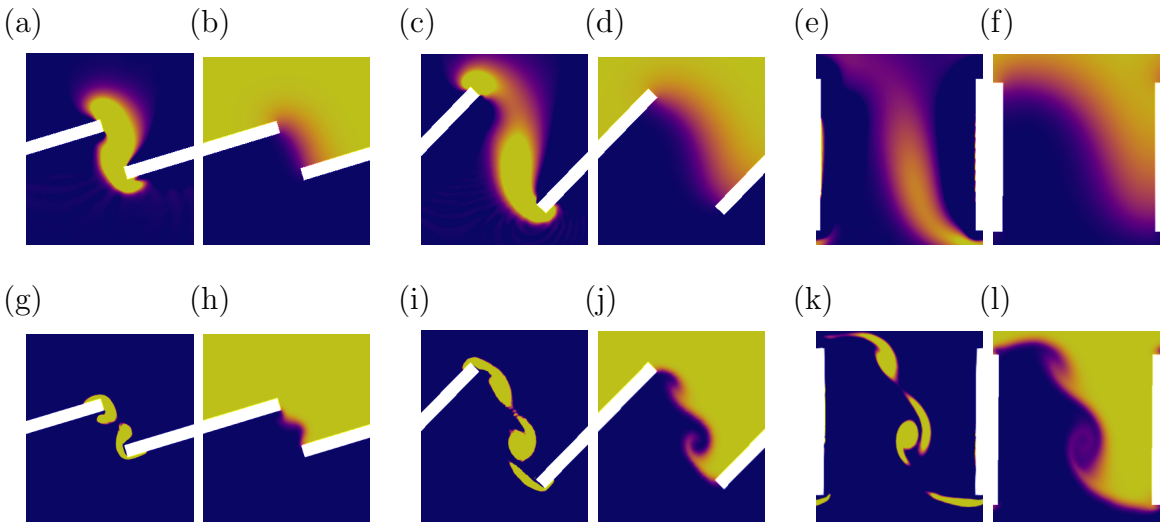

Fig.3 Composite images of the phase evolution of (left) iso contours of vorticity and (right) mass fraction of air during the opening of the blades, for the bi-gas configuration, for $\left[Re_{tip}^{LP1} \approx 50/Re_{tip}^{LP2} \approx 6\right]$ (upper line) and $\left[Re_{tip}^{LP1} \approx 1000/Re_{tip}^{LP2} \approx 130\right]$ (lower line). Colormap is kept constant and saturated for the sake of clarity for each opening time.

cores which remain connected to either the plunging or ascending blade tips by a vorticity filament associated with the shear layer. Moreover, the position of the vortices between the two co-rotating blades is constrained by the geometrical confinement which impings the displacement of the vortex cores, contrary to, *e.g.*, single rotating plate configurations [11]. By further increasing the Reynolds number, up to $Re^{LPi_{i=1,2}} \approx 2500$, iso-contours of vorticity now reveal the distortion of the shear layers connecting the vortex cores to the blade tips following a non monotonous shape. This new regime, referred to as regime 4, coincides with the roll-up of the starting vortices into more circular shapes. This might lead to an imminent separation of the vortex core from the shear layer, however limited by the previously evoked confinement effects. In this regime, the tangential velocity of the vortex core increases proportionally to the blade opening velocity, as a consequence of a noticeable increase of the vortex circulation while the vortex radius remains almost constant (Figure 2).

Figure 3 shows composite images of vorticity iso contours and air mass fraction for the bi-gas configuration and for two distinct opening velocities of the blades. In Figures 3(a)-(f) ($\left[Re_{tip}^{LP1} \approx 50/Re_{tip}^{LP2} \approx 6\right]$) the structure of the flow generated by the opening of the blades reveals different flow regimes depending on either the plunging or ascending tip blades, resulting from the different gas properties in LP1 and LP2, respectively. The flow structure resulting from the ascending motion of the blade tip traveling into LP2 chamber, filled with pure helium, promotes a regime 1-like flow. Indeed the Reynolds number based on the fluid properties in LP2 and on the velocity at the blade tip is approximately equal to 6. Contrarily, the structure of the flow which develops past the plunging blade tip moving into air in LP1 highlights a regime 2 pattern, in agreement with the Reynolds number at the blade tip, and with the previous analysis. At last, the iso contours of air mass fraction show a monotonous and quite diffuse shape of the gas interface since the relatively long opening time considered here leaves molecular diffusion imprint.

Contrarily, for $\left[Re_{tip}^{LP1} \approx 1000/Re_{tip}^{LP2} \approx 130\right]$ (Figure 3 (g)-(l)) where the opening time

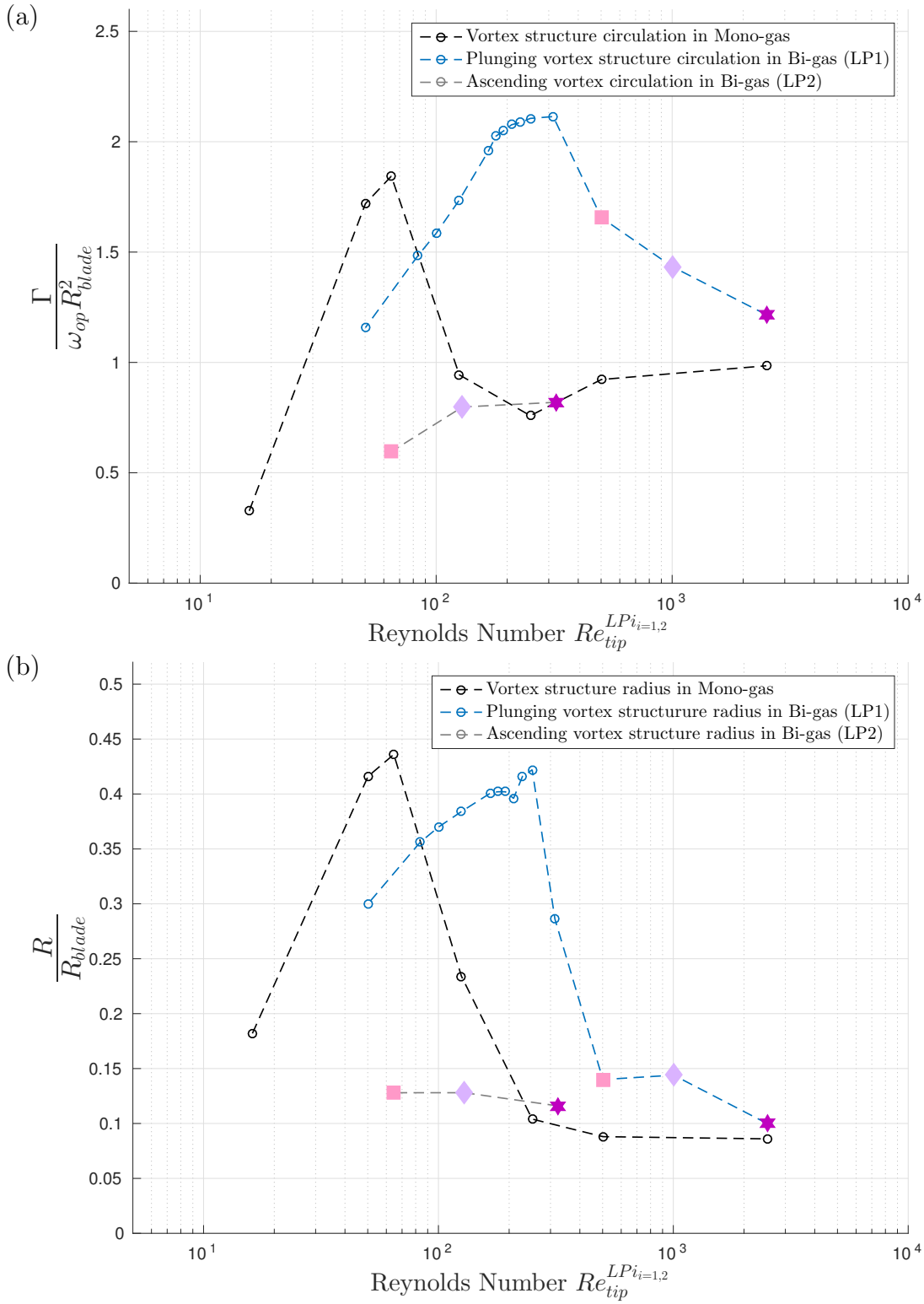

Fig.4 Evolution of (a) the normalized circulation and (b) radius of the vortex cores identified at the end of the opening phase of the blade, for mono-gas and bi-gas configurations, as a function of the Reynolds number $Re_{tip}^{LPi_{i=1,2}}$. Black dashed curve is for the mono-gas configuration. Blue/gray dashed curves are for plunging/ascending tip-generated vortices for the bi-gas configuration. In this configuration, pink squares are related to a blade opening time $t_{open} = 5ms$, light purple diamonds are for $t_{open} = 2.5ms$ and deep purple stars are for $t_{open} = 1ms$.

is 20 times shorter than for the previous case, the gaseous interface generated between air and helium at the end of the blades opening phase is weakly diffuse. Images of air mass fraction in Figure 3(h),(j),(l) exhibit a non monotonous shape, revealing the impact of the vortical flow. It is the result of the superimposing of regime 4-/regime3-like flow patterns past the plunging/ascending tips, respectively.

These results can finally be summarized into two different curves depicted in Figure 4, where the evolution of both the normalized circulation and radii are presented as a function of the Reynolds number $Re_{tip}^{LPi_{i=1,2}}$ for the mono-gas and bi-gas configurations. Three specific opening times for which the inception of a vortex structure at the ascending tip of the rotating blades is detected, are highlighted in the form of colored symbols. In particular, for a given opening time, the effect of the multi-gas flow on the distribution of the total amount of circulation (Figure 4(a)) between the plunging/ascending tip-generated vortical structures is well-observable when summing the circulations associated with pairs of similar symbols (gray and blue dashed curves). The circulation of the vortex core generated by the ascending tip in regime 3 (Figure 4(a), grey dashed curve) always remains lower than the one generated for the same opening time in a mono-gas configuration. On the contrary, the circulation of the vortex generated by the plunging tip, for the same opening time (Figure 4(a), blue dashed curve), is always quite larger than the one generated for the flow regime 4 in a mono-gas configuration when fixing the opening velocity of the blades. Interestingly enough, the total circulation of the tip vortices, i.e. the summation of the circulations obtained for the two vortices generated at the tip of the plunging and ascending blade tips, respectively, for different blade opening speeds, remains quite similar for both the mono-gas and bi-gas configurations. It reflects the influence of the density gradient on the distribution of a given amount of circulation into the two vortex cores. This total amount of circulation is imposed by the rotation of the blade, and distributes differently into these vortices since they originate from different flow regimes. Similarly, the independence of the radii to the Reynolds number is also clearly visible when comparing the values associated with identical symbols (Figure 4(b)). This is a well known feature for this range of Reynolds numbers where the flow is massively separated. Indeed for such configurations the size of the vortex cores is driven by the characteristic dimension of the object traveling in the fluid, in this case the rotating blades.

6 Discussion and conclusions

In this paper, a parametric study of the Richtmyer Meshkov Instability-dedicated initial conditions produced by an innovative experimental device has been conducted numerically. The aim was to characterize the generation of a fully-controlled and weakly diffused initial gaseous interface, that will further be impacted by an incident then reflected shock wave. The results demonstrate the ability of this experimental system to generate a well-defined gaseous interface with different shapes by varying its operating parameters, in particular the opening time of the blades constituting part of this device.

The various shapes highlighted by this study result from the occurrence of 4 specific flow regimes, ranging from a Stokes regime to a massively separated flow exhibiting a distorted shear layer connecting a starting vortex structure to its respective blade tip. These regimes have been deciphered first for a mono-gas configuration, then confirmed

for the bi-gas configuration. The inception of these various regimes depend on the local Reynolds number determined on the basis of the velocity at the tip of the blade and on the properties of the fluid the tip is traveling to. The originality of the flow pattern promoted by the opening of the blades in a bi-gas configuration comes from the concomitance of two different regimes occurring simultaneously for a given opening time, depending on the considered blade tip. This results from the different gas properties in which the plunging/ascending blade is moving in. Nevertheless, for regime 3 and regime 4, the radius of the starting vortices is almost constant for a large range of Reynolds numbers showing that the size of these structures is essentially driven by the geometry of the object. Contrarily, the total circulation imposed by the rotational motion of the blades, at a constant speed, experiences an unequal distribution amongst the two starting vortices. The influence of the density gradients imposed by the multi species explains most probably these observations. This should, however, be confirmed in further studies. It is also relevant to mention that the sum of the ascending and plunging vortex circulations, for a given opening speed, equals the sum of the circulations of the two similar vortices generated in a mono-gas configuration.

To conclude, the work presented here is of prime interest when investigating the sensitivity to the initial conditions of a turbulent mixing zone originated from a gaseous interface impulsively accelerated by a shock wave. In other words, if we want to confirm the persistence or the oblivion of the initial conditions on the late development of a turbulent mixing zone, it requires the precise determination of these initial conditions. This study is a step towards this goal.

Acknowledgements

This work is supported by CEA, DAM, DCRE under Grant No. CAJ-18-59/C33893, monitored by Dr. Denis Souffland. The authors gratefully acknowledge the computing center CALMIP for the computational resources provided under Grant P16034.

References

[1] R.D. Richtmyer, *Taylor instability in shock acceleration of compressible fluids*, Communications on Pure and Applied Mathematics. **13**, 2 (1960)

[2] E. Meshkov, *Instability of the interface of two gases accelerated by a shock wave*, Fluid Dynamics. **4**, 5 (1969)

[3] C. Mariani, M. Vanderboomgaerde, G. Jourdan, D. Souffland and L. Houas, *Investigation of the Richtmyer-Meshkov instability with stereolithographed interfaces*, Physical Review Letters. **100**, 25 (2008)

[4] K.P. Prestridge, P.M. Rightley, P. Vorobieff, R.F. Benjamin and N.A. Kurnit, *Simultaneous density-field visualization and PIV of a shock-accelerated gas curtain*, Experiments in fluids, **29**, 4 (2000)

[5] C. Weber, N. Haehn, J. Oakley, D. Rothamer and R. Bonazza, *Turbulent mixing measurements in the Richtmyer-Meshkov instability*, Physics of Fluids. **24**, 7 (2012)

[6] J.W. Jacobs, V.V. Krivets, V.Tsiklashvili and O.A. Likhachev, *Experiments on the RichtmyerMeshkov instability with an imposed, random initial perturbation*, Shock Waves. **23**, 4 (2012)

[7] G. Bouzgarrou, Y.Bury, S. Jamme, L.Joly and J.-F. Haas, *Laser doppler velocimetry measurements in turbulent gaseous mixing induced by the RichtmyerMeshkov instability: statistical convergence issues and turbulence quantification*, Journal of Fluids Engineering. **136**, 9 (2014)

[8] D.T. Reese, A.M. Ames, C.D. Noble, J.G. Oakley, D.A. Rothamer and R. Bonazza, *Simultaneous direct measurements of concentration and velocity in the Richtmyer-Meshkov instability.* Journal of Fluid Mechanics. **849** (2018)

[9] J.C.R. Hunt, *Vorticity and vortex dynamics in complex turbulent flows*, Transactions of the Canadian Society for Mechanical Engineering. **11**, 1 (1987)

[10] L. Ting & R. Klein, *Viscous vortical flows*, (Springer, 1991), v.374

[11] M.J. David, M. Mathur, R.N. Govardhan, J.H. Arakeri, *The kinematic genesis of vortex formation due to finite rotation of a plate in still fluid*, Journal of Fluid Mechanics, **839** (2018)